

The CALIPSO retrieved spatiotemporal and vertical distributions of AOD and extinction coefficient for different aerosol types during 2007–2019: A recent perspective over global and regional scales

Honglin Pan^{a,b}, Jianping Huang^{a,*}, Kanike Raghavendra Kumar^c, Linli An^a, Jinxia Zhang^a

^a Collaborative Innovation Center for Western Ecological Safety, College of Atmospheric Sciences, Lanzhou University, Lanzhou, 730000, China

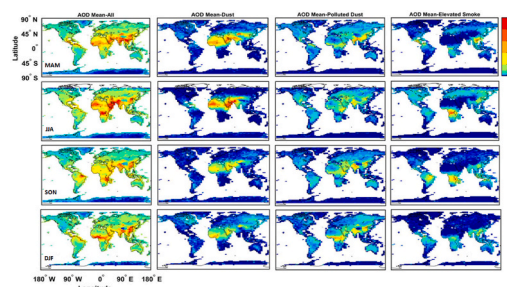
^b Institute of Desert Meteorology, China Meteorological Administration, National Observation and Research Station of Desert Meteorology, Taklimakan Desert of Xinjiang, Taklimakan Desert Meteorology Field Experiment Station of China Meteorological Administration, Xinjiang Key Laboratory of Desert Meteorology and Sandstorm, Key Laboratory of Tree-ring Physical and Chemical Research, China Meteorological Administration, Urumqi, 830002, Xinjiang, China

^c Department of Physics, Koneru Lakshmaiah Education Foundation (KLEF), Vaddeswaram, 522502, Guntur, Andhra Pradesh, India

HIGHLIGHTS

- The CALIPSO retrieved global AOD for all aerosol types showed a maximum in summer.
- The spatiotemporal changes in AOD were observed for all types of aerosols.
- The biggest difference in total AOD between land and ocean areas occurred in summer.
- Annual variations of AOD are relatively stable for all aerosol types.

GRAPHICAL ABSTRACT



ARTICLE INFO

Keywords:

CALIPSO
AOD
Extinction coefficient
Aerosol types
Spatiotemporal and vertical distributions

ABSTRACT

In the present study, we investigated the global climatology of the spatiotemporal and vertical distributions of aerosol optical properties for different aerosol types, mainly including total aerosols (All), desert dust (DD), polluted dust (PD), and elevated smoke (ES). The data used for the study is derived from the Cloud-Aerosol Lidar and Infrared Pathfinder Satellite Observations (CALIPSO) for Research and Application. We found that the seasonal distribution of the global mean aerosol optical depth (AOD) of All type in the land area are in the order JJA (0.157) > MAM (0.134) > DJF (0.127) > SON (0.124). This is attributed to the more frequent sand and dust activities over the Taklimakan Desert and the Sahara Desert in MAM and JJA. Owing to the transportation of DD, ES, and PD from the aerosol source, the ocean areas (especially for downwind regions) present the high AOD, and with the same seasonal distribution trend as in the land area. Also, the mean extinction coefficient (EC) for all aerosols decreases with the increase of height in all seasons for both hemispheres. The maximum mean EC for All aerosols is 0.0102 km^{-1} (0.016 km^{-1}) during the day (night) in DJF (JJA) in the northern hemisphere, while the

* Corresponding author.

E-mail address: hjp@lzu.edu.cn (J. Huang).

<https://doi.org/10.1016/j.atmosenv.2022.118986>

Received 12 October 2021; Received in revised form 29 January 2022; Accepted 2 February 2022

Available online 5 February 2022

1352-2310/© 2022 Elsevier Ltd. All rights reserved.

maximum is 0.006 km^{-1} (0.008 km^{-1}) during the day (night) in JJA (SON) in the southern hemisphere. Also, the occurrence of frequencies of DD, PD, and ES aerosols are distributed throughout the entire troposphere in all seasons, but the clean marine (CM) and polluted continent (PC) are mostly below 3 km.

1. Introduction

The accurate understanding of the physical and optical properties of different aerosol types at global and regional scales is essential to assess and study the impact of aerosols on climate change (Charlson et al., 1992; Carslaw et al., 2013; Luo et al., 2013; Nan and Wang, 2018; Mehta et al., 2018; Sogacheva et al., 2020). Atmospheric aerosols can be transported to far distant places away from their sources in the troposphere, which, in turn, changes their spatial distribution of optical properties (Chen et al., 2010; Huang et al., 2008, 2015a, b; Hu et al., 2019a). It is important to infer their transport mechanism, emission characteristics, and a columnar rise of aerosols through the vertical structure and spatial distribution of aerosols (Uno et al., 2008; Winker et al., 2013; Jia et al., 2015; Zhang et al., 2019; Kumar et al., 2018). In particular, the uncertainty in the simulated transport process is one of the main factors in predicting aerosol distribution diversity by the global aerosol model (Uno et al., 2001; Textor et al., 2006; Huang et al., 2008; Hu et al., 2019b; Fan et al., 2020). Therefore, the global observation of aerosol optical properties and their spatial and vertical structure is very important to evaluate their role in atmospheric dynamics. Furthermore, the global vertical distribution of tropospheric aerosols is, particularly, valuable for the evaluation of global aerosol models, because it is a combination of aerosol emission, vertical uplift, exchange intensity, and removal process.

To understand the vertical structure and optical properties of aerosol distribution in the atmosphere, many experts and scholars have carried out some regional studies in different regions of the world using the ground-based and space-borne LiDAR (LIght Detection And Raging) (Menzies and Tratt, 2002; Mona et al., 2006; Huang et al., 2007, 2009, 2010, 2014; Solanki and Singh, 2014; Mehta et al., 2018; Liu et al., 2019; Shikwambana and Sivakumar, 2018; Wang et al., 2020). The ground-based LiDAR can realize the repeated and accurate detection of aerosol characteristics at a single site, while the satellite can realize irreplaceable and continuous space-time coverage observation, can provide the global spatial and temporal distribution of aerosols. Hence, the Cloud-Aerosol Lidar with Orthogonal Polarization (CALIOP), which is onboard NASA's platform i.e., Cloud-Aerosol Lidar and Infrared Pathfinder Satellite Observations (CALIPSO), has been gathering the information of aerosol-cloud through their vertical distributions over more than a decade, since from the late of 2006 (Mehta et al., 2018; Shikwambana and Sivakumar, 2018; Pan et al., 2021). Earlier, numerous researchers (Mehta et al., 2018; Shikwambana and Sivakumar, 2018; Pan et al., 2019, 2020, 2021) used the CALIOP data to evaluate the regional and global vertical characteristics of aerosols over a specific domain of interest.

In this context, it is reported that the CALIPSO can observe aerosols on bright surfaces and under thin clouds, as well as during clear sky conditions (Winker et al., 2006), which is very beneficial to the separation of aerosols and clouds. Later, Liu et al. (2008), who first proposed the global distribution of dust aerosol height with its spatiotemporal resolution. Also, Huang et al. (2008) revealed that the combination of different dust sources formed a double or multi-layer dust structure over East China and the West Pacific Ocean using the CALIPSO and surface measurements. Further, Yu et al. (2010) studied the seasonal variations of aerosol vertical distribution based on the one-year CALIOP data (i.e., from June 2006 to November 2007). It is also found that the geographical pattern and seasonal variation of AOD observed by the CALIPSO are consistent with the Goddard Chemistry Aerosol Radiation and Transport (GOCART) model simulation and the Moderate resolution and imaging spectroradiometer (MODIS) inversion (Filonchik et al.,

2020), especially in the near-source area, but the AOD levels vary in most areas. Further, Schuster et al. (2012) provided climatology for the Lidar ratio of dust from the CALIPSO over the well-established AERONET sites. In yet another study by Winker et al. (2013), they described the three-dimensional distribution of global tropospheric aerosols using the 6-year CALIPSO Level-3 aerosol products. The results showed that the vertical distribution varies with seasons because the source intensity and transport mechanism are significantly different. Besides, Mehta et al. (2018) utilized the global CALIPSO level-3 nighttime Standard-V3-00 All-Sky data products to discuss the columnar aerosol optical properties combined with vertical properties of different aerosol types during 2006–2016.

Recently, Nan et al. (2018) analyzed the inter-annual variation of extinction in Taklimakan Desert aggregated of dust aerosols in different altitudes using the CALIPSO sounding data during the spring (MAM) season from 2007 to 2016. However, their work mainly focused on the old version of inversion data for CALIPSO, and the research period is relatively short (Huang et al., 2013). Despite previous efforts made by several researchers to evaluate aerosol vertical distributions, there still exists a lack of assessment of global aerosol diurnal changes (Marinou et al., 2017; Mehta et al., 2018; Tandule et al., 2020). In this paper, the newest aerosol profile of CALIPSO level-3 Version-4.20 All-Sky Standard data is utilized for more than a decade of data collected for the years during 2007–2019 are investigated over the global and regional scales.

The present study aims to analyze qualitatively the climatology of spatiotemporal distribution of different aerosol types observed during 2007–2019 based on the CALIPSO data. The study also provides the comprehensive analysis of aerosols for the researchers to conduct the related study, for example, comparison between satellite retrievals and model. Further, the study is desired specifically to improve and constrain the modeling in atmospheric dynamics and climate change over the globe. The objectives of the present study are designed as follows: (1) to analyze annual and seasonal variations of the vertical and spatiotemporal distributions of aerosol optical properties and its types on regional and global scales; and (2) to evaluate and understand the diurnal and zonal changes of the vertical distribution of different aerosol types.

2. The CALIPSO instrument

The release of the CALIPSO Lidar level-3 version 4.20 tropospheric aerosol profile product marks several improvements over the prior version 3.0. Most importantly, the new level-3 products are constructed from version 4.2 level-2 input data which are the highest quality and most sophisticated of all CALIOP level-2 data products. The new level-3 quality screening procedures have been implemented to improve the quality of statistics reported by the product. Minor changes to science data set names and bug fixes are also included in the newest version 4.20. In the present study, we used the recently released CALIPSO level-3 version 4.20 aerosol vertical profile data products (newly released in September 2019), a globally gridded monthly 5-km aerosol profile product derived from the level-2 CALIPSO version 4.2. The level-2 aerosol profile data are quality screened and then aggregated onto a global $2^\circ \times 5^\circ$ latitude-longitude grid. The vertical resolution is 60 m from -0.4 to 12.1 km above mean sea level (AMSL), with a total of 208 layers. Averaged profile data after quality screening are reported for all-aerosol (regardless of its type) and mineral dust aerosol only. The classification of dust is based on the aerosol type flags in the level-2 profile data. Aerosol type information from level-2 data is also reported in level-3 as histograms of aerosol type for each latitude/longitude/altitude grid

cell, including all seven aerosol types. Depending on the sky condition (combined, i.e., cloud-free, or all-sky) and lighting condition (daytime or nighttime), there are four different types of level-3 data files. The primary data variables, include, are spatial and vertical distributions of the aerosol extinction coefficient (EC) and its associated types, and aerosol optical depth (AOD).

In the present work, we used the All-sky data and the period of data used is considered from January 2007 to December 2019. Because cloud-free products also eliminate aerosol samples in the process of removing cloud samples from the entire vertical profile, it will lead to the reduction of aerosol samples and may further underestimate the values of aerosols. Therefore, we chose the All-sky product to retain complete aerosol information. The CALIPSO nighttime data at 532 nm only is used, because of their better signal-to-noise ratio (SNR) compared to the daytime measurements, to analyze global/regional climatological and seasonal variations of the vertical distribution of aerosol optical properties and its types. The seasonal vertical profiles of aerosol EC are calculated based on average, i.e., the average of all grid cells.

3. Results and discussion

3.1. Global spatial distribution of AOD over land and ocean

To better demonstrate the difference in the global spatial distribution of aerosols observed over the land and ocean samples (land and ocean area), we have divided the global key regions into eight lands (red box) and six ocean (blue box) regions (Fig. 1). In general, the main remotely sensed geophysical quantity, being the total column AOD, is defined as the vertically integrated extinction due to aerosol scattering and absorption. Further, the study has separated the land (Fig. 2) and ocean (Fig. 3) samples to better characterize the variations of the global distribution of aerosols and their types for four seasons. Table 1 presents the quantitative estimates of 13-year averaged-global AOD over land and ocean samples for all seasons. The CALIPSO measurements are divided into daytime and nighttime conditions, and we have chosen here the nighttime data to detect optically thin layers (see Figs. 2 and 3). Besides, the aerosol types are divided into seven classes, where, we emphasize the total aerosols (All), desert dust (DD), polluted dust (PD), and elevated smoke (ES) as only provided by the CALIPSO. It is mentioned here that 'All' means total aerosol loading; mineral dust is classified by the CALIOP as either 'Dust' which means pure dust or 'Polluted Dust' represents dust mixed with smoke or other non-depolarizing aerosols; whereas, the 'Elevated Smoke' indicates

aerosols produced from biomass burning/forest fires (Winker et al., 2013; Mehta et al., 2018). Besides, DD, PD, and ES are the three major aerosol types present in All aerosol types. All aerosol loading can completely reflect the global distribution of total aerosol AOD as shown in Figs. 2 and 3. The CALIPSO level-3 datasets only show the extinction coefficient (EC) and AOD for three classes of aerosol types and All aerosol loading as well. Hence, the AOD and EC of the other four types aerosol are not considered in this manuscript.

Fig. 2 shows the global land sample distribution of AOD for different aerosol types (include All, DD, PD, and ES) for four seasons. First, we found that the distributions of AOD of are mainly over Asia and Africa, especially in western Asia (ASW), eastern Asia (ASE), the Taklimakan Desert, and the Sahara Desert in spring (MAM) and summer (JJA). Also, the AOD found during autumn (SON) and winter (DJF) is less than that noted in the MAM and JJA seasons. In SON, high AOD is distributed in SA, northern Africa (AFN), southern Africa (AFS), ASW, ASE, and Australia (AUS). Whereas the high AOD during DJF is distributed in Africa, ASW, ASE, Boreal (BOR), and AUS, especially at the junction of AFS and AFN. Second, with the distribution of global land samples of AOD for DD type, it is evident that the activity of sand and dust particles in the Taklimakan Desert (TD), the Sahara Desert (SD), and the NA are more frequent during the MAM and JJA seasons where the concentration of DD type of aerosols was higher in the TD than the SD. This is agreement and like what have been reported earlier by Mehta et al. (2018), Dayan et al. (2008), Rashki et al. (2014), and Wang et al. (2008) in their studies using different sensors and different satellite products.

As shown in Table 1, for AOD of All types, the global distribution of seasonal characteristics of AOD over the land for the period 2007–2019 were noticed in the decreasing order as follows: JJA (0.157) > MAM (0.134) > DJF (0.127) > SON (0.1242). Our findings are nearly consistent with that reported by Mehta et al. (2018) over the globe. While for AOD of DD type, has the same variation in trend as JJA (0.050) > MAM (0.047) > DJF (0.026) > SON (0.024). It is found that higher proportion of AOD for DD in MAM (34.97%) and JJA (31.83%) in the global AOD distribution in the land. ES or PD aerosol type, the existence of dust and smoke makes the PD aerosol type existence as well, which covers almost the whole land area. The global distribution of mean AOD for PD type is in the order of DJF (0.034) > JJA (0.029) > MAM (0.029) > SON (0.028). Also, for the ES aerosol type, it is widely distributed in NA, SA, Europe, AFS, and ASW (especially for southeast China, mainly due to anthropogenic emissions) in JJA. Among them, the aerosol pollution of rising smoke in Europe is caused by forest fires; and in NA, where fossil fuel burning and industry generated aerosols are or transported (if the AOD is lower) most common (Huang et al., 2013;

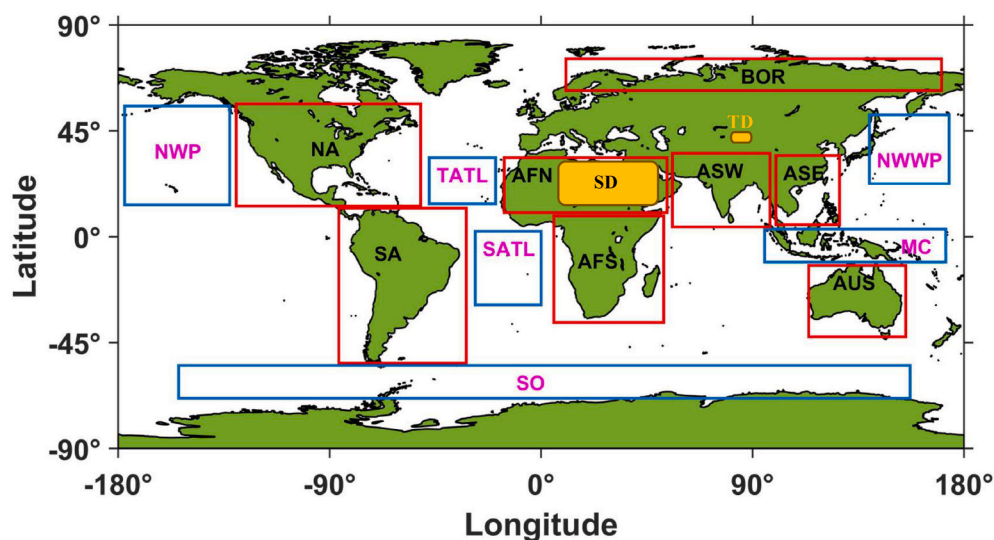


Fig. 1. Globally eight lands (red box) and six ocean (blue box) regions are defined in the present study as North America (NA), South America (SA), Northern Africa (AFN), Southern Africa (AFS), Boreal (BOR), Western Asia (ASW), Eastern Asia (ASE), Australia (AUS); Northwest Pacific (NWP), Tropical Atlantic (TATL), South Atlantic (SATL), Southern Ocean (SO), Northwest Western Pacific (NWWP), and Maritime Continent (MC). Besides, the. (For interpretation of the references to colour in this figure legend, the reader is referred to the Web version of this article.)

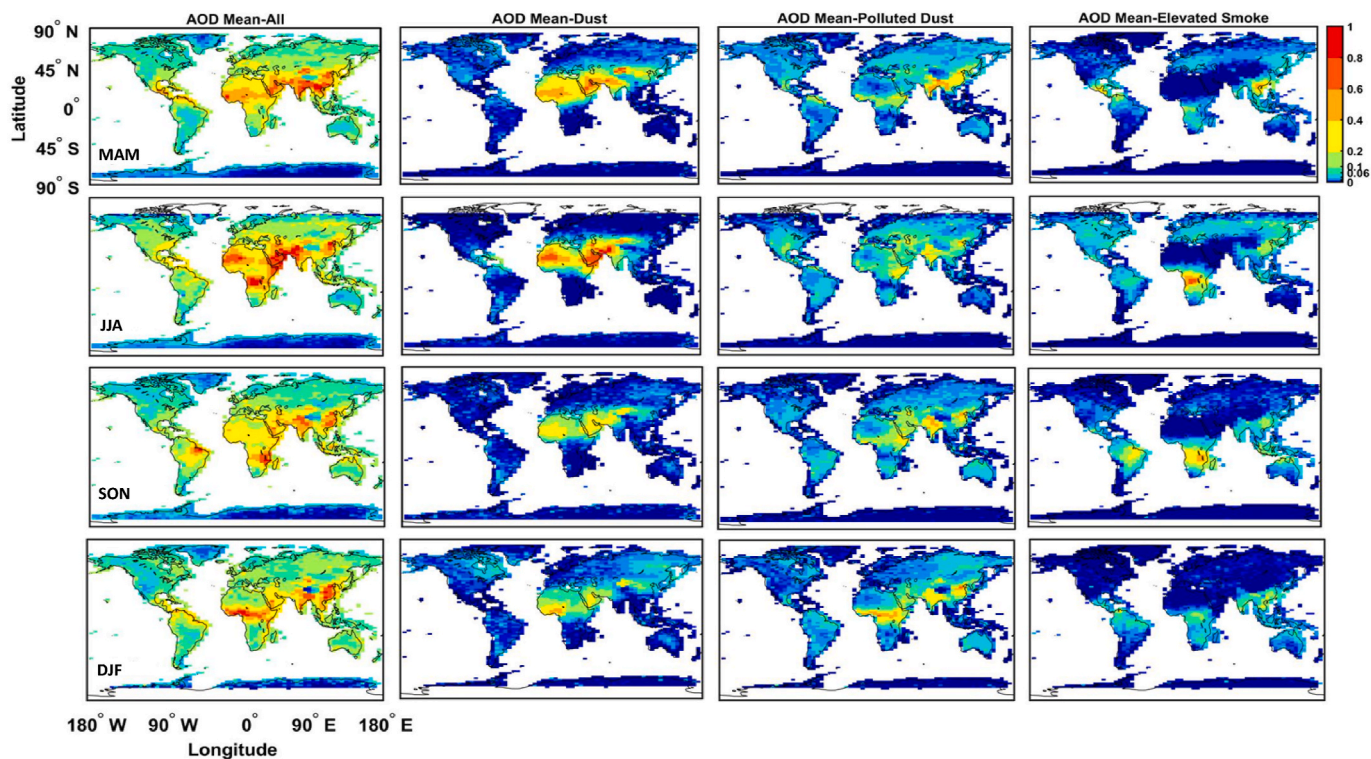


Fig. 2. Global distribution of mean AOD for All, dust, polluted dust, and elevated smoke for land-only data in four seasons based on the CALIPSO nighttime data observed during 2007–2019.

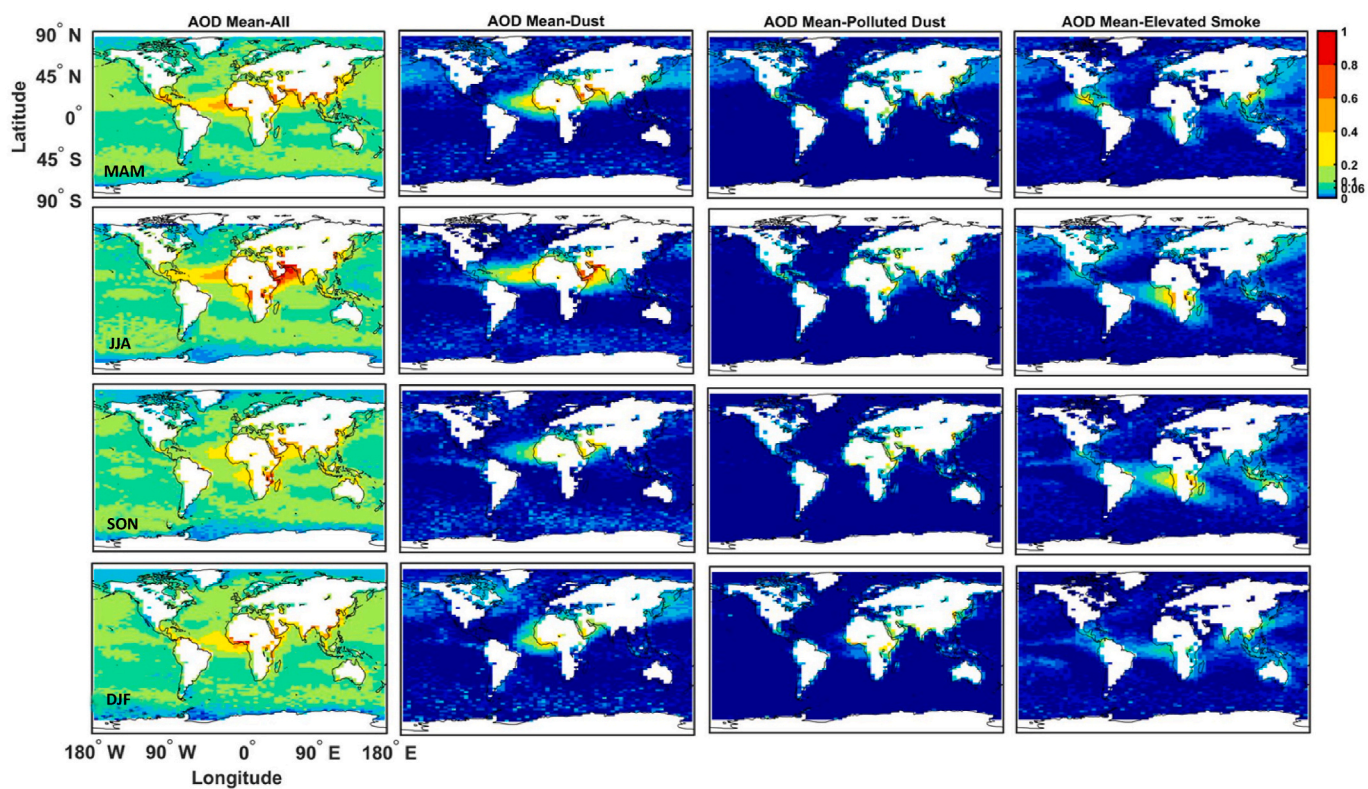


Fig. 3. The representation is the same as shown in Fig. 2, but for the ocean-only data.

Table 1

The global statistical means of CALIPSO retrieved AOD with their percentage contributions (shown within the parenthesis) for All, DD, PD, and ES type of aerosols for land-only (represented values in bold) and ocean-only during nighttime in all seasons during 2007–2019.

Season	Land only/Ocean only			
	All_AOD	DD_AOD	PD_AOD	ES_AOD
MAM	0.1341/ 0.1053	0.0469/0.0155 (14.72%)	0.0292/0.0072 (21.77%)	0.0154/0.0103 (9.78%)
JJA	0.1574/ 0.1126	0.0501/0.0197 (31.83%)	0.0293/0.0065 (18.61%)	0.0262/0.0131 (11.63%)
SON	0.1242/ 0.0975	0.0238/0.0090 (19.16%)	0.0279/0.0057 (22.46%)	0.0215/0.0119 (17.31%)
DJF	0.1272/ 0.0986	0.0257/0.0104 (9.23%)	0.0336/0.0063 (1.92%)	0.0122/0.0074 (12.21%)
		(20.20%) (10.55%)	(26.42%) (6.39%)	(9.59%) (7.51%)

Kumar et al., 2014; Kaskaoutis et al., 2011; Roberts et al., 2009); while the smoke aerosol pollution in South America, Southern Africa, and Asia attributed to biomass burning (Mehta et al., 2018; Butt et al., 2016; Das et al., 2017; Heilman et al., 2014; McKendry et al., 2011; Vaughan et al., 2018). The ES aerosol type is widely distributed in SA, AFS, Southeast China, Amazonia, Indonesia, and AUS during the SON and DJF seasons. The global land samples distribution of mean AOD for ES is in the decreasing order as: JJA (0.026) > SON (0.021) > MAM (0.015) > DJF (0.012). To sum up, the main contribution of aerosols in MAM (34.97%) and JJA (31.83%) comes from the DD type, whereas the PD type of aerosols dominated in SON (22.46%) and DJF (26.42%). There are more aerosols caused by industrial development, forest fires, and human activities in SON and DJF.

The global distributions of mean AOD for DD, PD, ES, and All aerosol types during 2007–2019 for ocean samples are shown in Fig. 3. The global AOD distribution for the ocean samples is captured for All aerosols, which has the same trend as land samples for the four seasons (JJA (0.113) > MAM (0.105) > DJF (0.099) > SON (0.097)). The AOD distribution for ocean samples is mainly centered in the northwestern Pacific (NWP), Tropical Atlantic (TATL), South Atlantic (SATL), Southern Ocean (SO), northwest Western Pacific (NWWP), and Maritime Continent (MC). For DD type, moderate (lower) AOD is found in the MAM and JJA (SON and DJF) seasons associated with the outflow of the Sahara Desert into the TATL and ASW. It is worth noting that there is a weak AOD in MAM and DJF with DD outflow into the NWP and NWWP. However, the PD showed lower AOD only in MAM associated with DD and smoke is mixed outflow into NWP and NWWP. For the ES type, the AOD associated with AFS smoke outflow into the SATL in JJA and SON. Except for this region, ASE, NWWP, and MC also showed distinct AOD for ES in all seasons are related to industrial development and human activities or due to transport from other regions (Mehta et al., 2018). It should be noted that the contribution of DD for the ocean samples is the largest in MAM (14.72%), JJA (17.50%), and DJF (10.55%), and that of ES is the largest in SON (12.21%). In general, the seasonal proportion of AOD contributed by DD, PD and ES aerosol types over land is MAM (68.22%) > JJA (67.09%) > SON (58.93%) > DJF (56.21%), while it is JJA (34.90%) > MAM (31.34%) > DJF (24.45%) > SON (23.36%) over the ocean.

3.2. Global vertical distribution of occurrence of frequencies for different aerosol types

To characterize the vertical distribution of the occurrence of frequencies of different aerosol types, we calculated frequency of occurrences of each aerosol type by dividing the number of aerosol type samples to the total number of CALIPSO measurements within each vertical layer. We divide the world into the northern and southern

hemispheres (i.e., NH and SH) for detailed discussion, aiming to explore the differences in the probability of occurrence of frequencies of different aerosol types in the NH and SH for each season. Generally, the CALIPSO detects more aerosol samples during nighttime rather than daytime, especially in the middle to upper troposphere, so we just choose nighttime data in the present study. Fig. 4 shows the vertical profile of the occurrence of frequencies of each aerosol type in each season for NH and SH. In NH, the occurrence of frequencies of each aerosol type has depicted large seasonal variations. The DD aerosol type is the most dominant type detected at 2–6 km in all seasons, except DJF when PD type (a mixture of smoke and dust (Omar et al., 2009; Huang et al., 2013)) dominates. Besides, the DD and PD types are the dominant ones detected at 6–12 km during MAM and DJF seasons; whereas the ES is the dominant type detected at 6–12 km during JJA and SON seasons. The frequency of occurrences of the ES type increased rapidly in all seasons below 2 km. However, the aerosol occurrence of frequencies has small seasonal variations in the SH. The ES dominates about 2–8 km nearly in all seasons, while PD is the secondary dominant type. Furthermore, the clean marine (CM) dominates below 2 km in all seasons. In MAM (JJA and DJF), the DD type prevails above 8 km (10 km and 9 km), and the ES type is the secondary dominant one. The ES type appears as the most prevailing aerosol type detected from 2 km to 12 km in DJF, while the DD is the secondary dominant type above 8 km. From the above analysis, we can see that the complexity of seasonal variations of aerosol types reflects the significant impacts of both emissions from biomass burning and desert dust on the aerosol composition in NH and SH regions. Besides, the CM aerosol type appears to be the dominant type detected below 2 km in both NH and SH due to a large oceanic area in this domain (Huang et al., 2013). Hence, it is understood that the DD, PD, as well as ES, are the dominant aerosol types at nearly all levels in NH and SH regions.

3.3. Latitude-altitude distributions of the global aerosol extinction coefficient

To illustrate the contrasting differences of the various aerosol types over the NH and SH regions, we presented the vertical distribution of mean aerosol EC during daytime and nighttime. Figs. 5–8 shows the latitude-altitude (zonal) distributions of global aerosol EC derived from the CALIPSO for All, DD, PD, and ES aerosol types during the daytime and nighttime for four seasons during 2007–2019. To ensure the validity of the value and effectively express the vertical distribution of different types of aerosols in different seasons, we limit the value to 0.001–0.5 km^{-1} . It is evident from Fig. 5 that the mean aerosol EC for All types of aerosols generally, the EC decreases with the increase of height in all seasons over NH. High concentration aerosols are mainly concentrated in the boundary layer, and the zonal distribution of EC decreases with the increase of latitude, which may be related to the source emission of aerosols, such as the global desert belt at 0–40°. It is evident that the dust concentration is consistent with the locations of the Sahara Desert and the Taklimakan Desert (Fig. 6), as they are the main source areas of DD. In DJF, the aerosol lift height is lower than that in the other three seasons, which is related to the weak atmospheric convection in DJF. In the SH, the aerosol lifting height is lower than that in the NH, mainly because the ocean coverage area in the southern hemisphere is larger than the land area, mainly CM aerosol. Furthermore, the maximum mean aerosol EC value is 0.010 km^{-1} observed during the day in DJF, while the mean aerosol EC in all seasons during the night is greater than that of the day (Table 2). The reason is that the nighttime data has better SNR compared to the daytime measurements. Moreover, the maximum mean aerosol EC is 0.006 km^{-1} observed during the day in JJA where the mean EC during the night is greater than that of the day (Table 2). Also, the latitudinal distribution and vertical distribution of mean aerosol EC in NH and SH regions revealed that the maximum particle concentrations are confined at lower altitude regimes. Below 2 km, the aerosol signals gradually decrease with altitude and increase in latitude

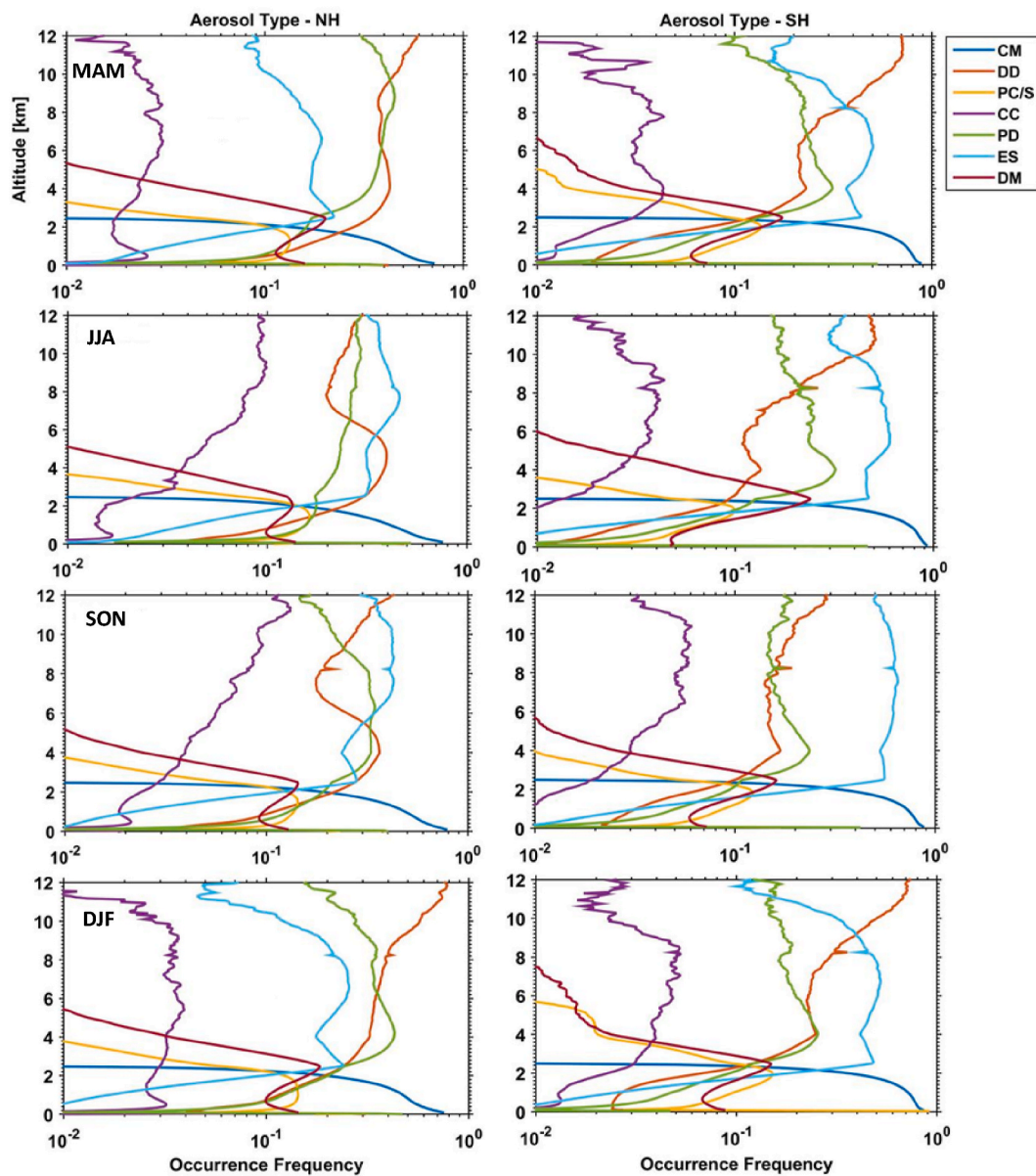


Fig. 4. Seasonal vertical profiles of occurrence frequencies of each aerosol type for the period 2007–2019 based on the CALIPSO nighttime observations over the Northern (NH; left column panels) and Southern (SH; right column panels) Hemisphere regions. The abbreviation of aerosol types represents clean marine (CM), desert dust (DD), polluted continental/smoke (PC/S), clean continental (CC), polluted dust (PD), elevated smoke (ES), and dusty marine (DM).

because the aerosols are transported from the sources (Mehta et al., 2018). Due to the large land area, more population, and intensive human activities in the NH, the total aerosol concentration is extremely higher than that in the SH.

We can see that the contribution of DD to All aerosols is the largest as mentioned before. During the MAM and JJA, the maximum values of mean aerosol EC were found as 0.006 km^{-1} and 0.004 km^{-1} observed in the night (Table 2). This shows that the high value of mean aerosol EC due to dust particles is observed over the global dust belt. Correspondingly, the PD concentration is the highest at $20\text{--}40^\circ \text{ N}$ and the height is less than 2 km in SON and DJF. Besides, the low values were found for DD, PD, and ES in the SH, which are hardly noticeable at higher altitudes and latitudes. It is worth noting that the maximum mean value of ES in all seasons appears at the height of 3 km in the NH, and 2.5 km in the SH. In general, the mean aerosol EC during nighttime in JJA over the NH is greater than those in other seasons, while the EC in SON over the SH is the highest (except for PD, shown in Table 2).

3.4. Annual variations of mean AOD for different aerosol types

In this section, we examine the global annual mean (with standard deviation) variations of AOD for All, DD, PD, and ES aerosols during the day and night for the period 2007–2019. It is mentioned that due to the lack of data in February 2016, there is a discontinuity in Fig. 9. The inter-annual variations of global aerosol AOD for the night and during the day show a decreasing trend. The AOD during the night is almost greater than 0.1, while it is found opposite for the day. Besides, the annual variation and daily range for mean AOD of DD compared with All aerosols are smaller. Interestingly, the annual and daily mean AOD of All and DD type of aerosols have followed the same trend during 2007–2019, showing obvious seasonal variation, and the daily variation of DD type is the smallest. However, the changing trend of daytime and nighttime is the same. It can be inferred that DD aerosol particles play a dominant role in the global total aerosol loading. For PD and ES aerosol types, the deviations are found smaller in low AOD aerosol types. Furthermore, the daily range of ES was greater than that of PD, and the

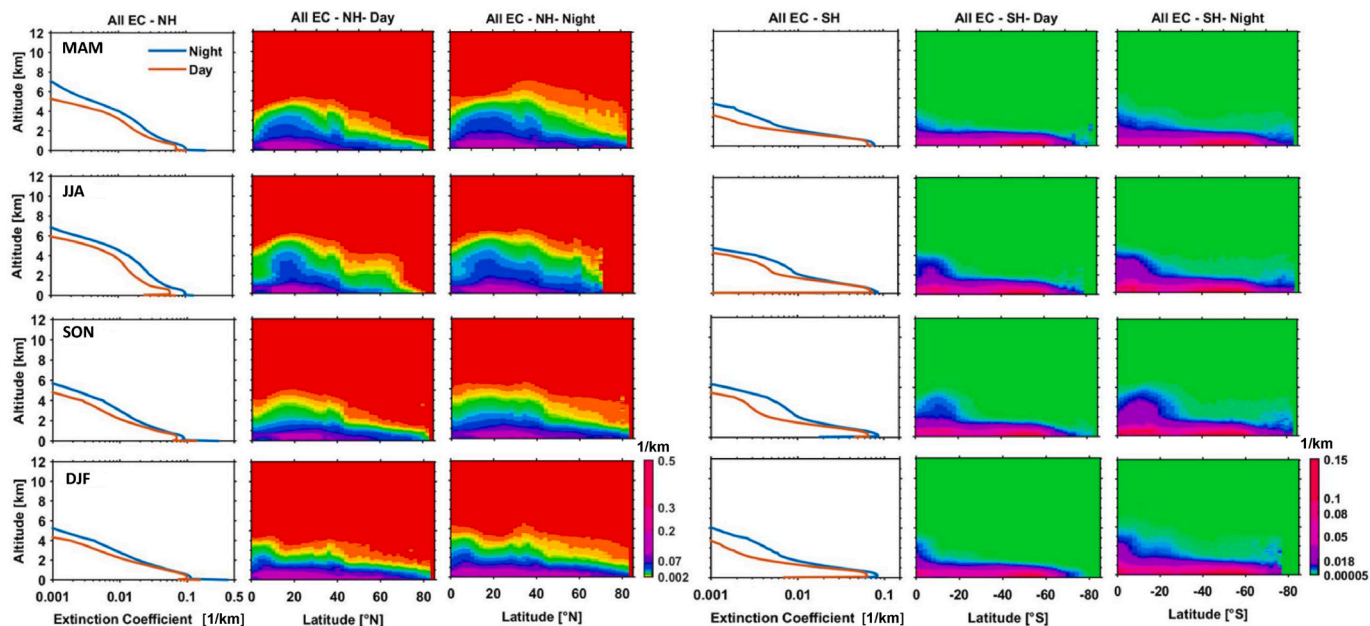


Fig. 5. The CALIPSO derived vertical profiles and zonal (latitude-longitude) distributions of total extinction coefficient (EC) for All aerosol types during the day and night in four seasons from 2007 to 2019 over Northern (NH; left three columns) and Southern (SH; right three columns) Hemisphere regions.

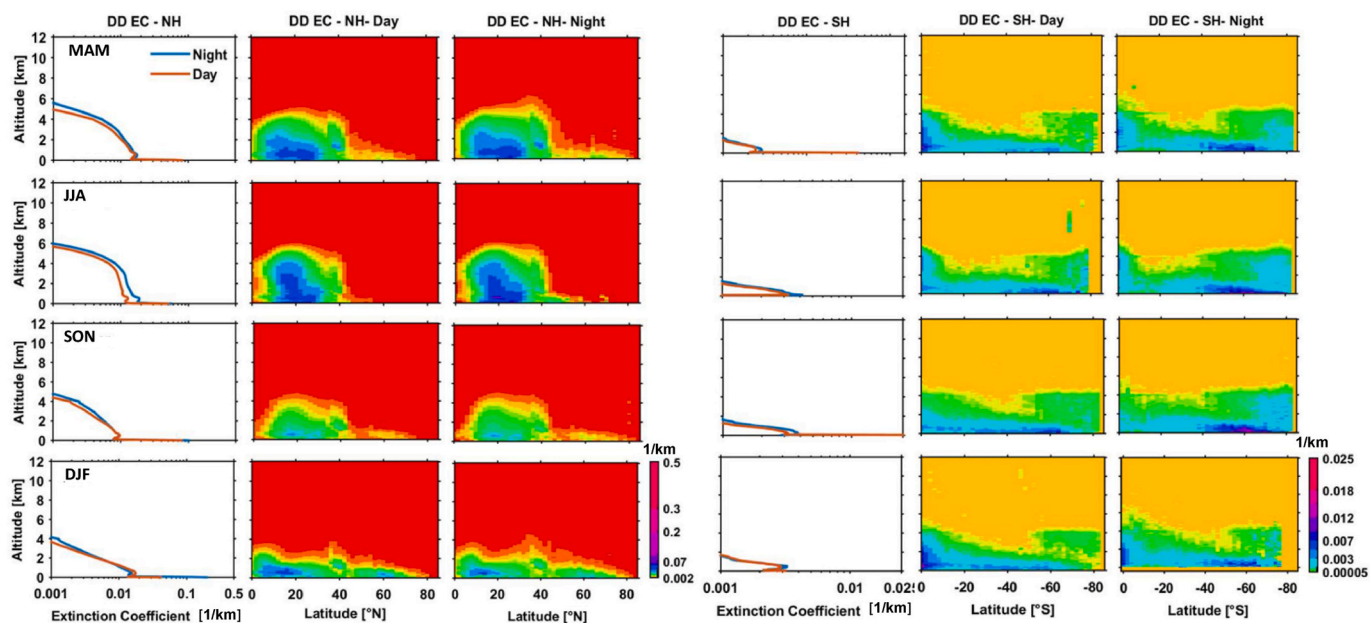


Fig. 6. The representation is the same as shown in Fig. 5, but for the EC due to desert dust (DD) aerosol type.

annual mean AOD of PD and ES during the day and night are stable, which has not found an obvious change in the trend during 2007–2019 (Fig. 9 and Table 3). For the AOD of DD, PD, and ES aerosol load, DD type is the largest contribution rate among the three aerosol types followed by PD, and ES is the least. In general, the annual variation of mean AOD during day and night is relatively stable, and the changing trend is not obvious for all aerosol types.

4. Summary and conclusions

In the present study, we investigated the spatiotemporal and vertical distribution of aerosol optical properties across the globe using the newest level-3 version 4.20 Standard All-Sky CALIOP datasets for the

period 2007–2019. For the global land samples, the distribution of mean AOD for All aerosols were observed in the order as JJA (0.157) > MAM (0.134) > DJF (0.127) > SON (0.124). We further observed that the activity of sand and dust in TD, SD, and northern Africa are more frequent during MAM and JJA seasons. Whereas the concentration of sand and dust in the Taklimakan Desert is higher than in the Sahara Desert in MAM (opposite in JJA). The main contribution of aerosols in MAM (34.97%) and JJA (31.83%) comes from the DD aerosols, whereas it is from the PD type in SON (22.46%) and DJF (26.42%). Furthermore, the global distribution of mean AOD of ocean samples for All aerosols followed a similar trend as the land samples in all seasons. Also, the seasonal proportion of AOD contributed by DD, PD and ES for land samples was observed as: MAM (68.22%) > JJA (67.09%) > SON

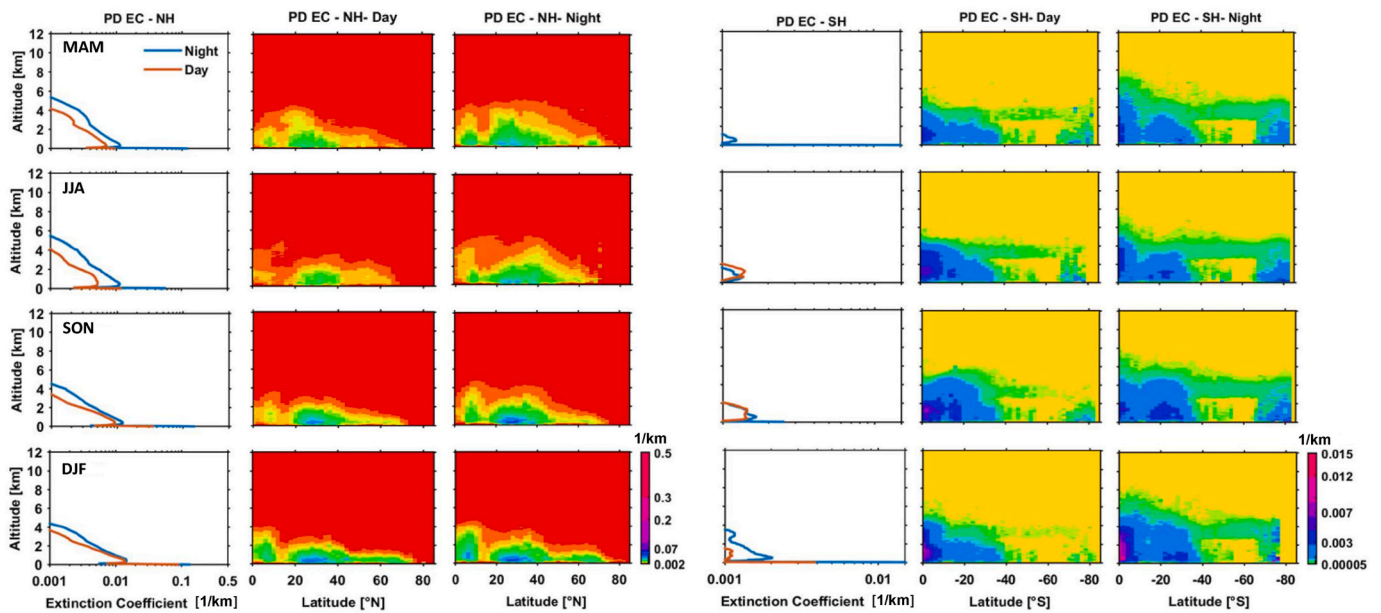


Fig. 7. The representation is the same as shown in Fig. 5, but for the EC due to polluted dust (PD) aerosol type.

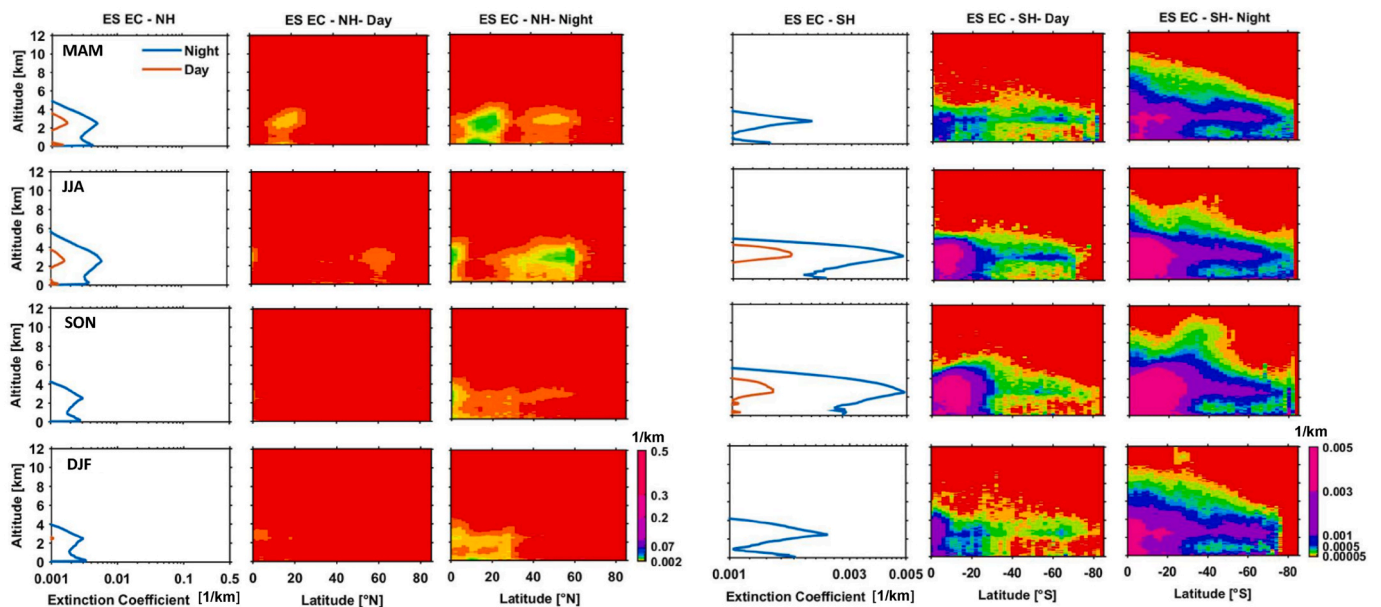


Fig. 8. The representation is the same as shown in Fig. 5, but for the EC due to elevated smoke (ES) type of aerosols.

Table 2

The CALIOP derived mean aerosol extinction coefficient (EC) for All, DD, PD, and ES aerosol types during daytime and nighttime for four seasons over the Northern (represented values in bold) and Southern Hemispheres during 2007–2019.

Aerosol Type	Northern Hemisphere/Southern Hemisphere - Mean EC							
	MAM		JJA		SON		DJF	
	Day	Night	Day	Night	Day	Night	Day	Night
All	0.0095 /0.0053	0.0139 /0.0067	0.0089 /0.0065	0.0162 /0.0079	0.0080 /0.0058	0.0117 /0.0083	0.0102 /0.0049	0.0129 /0.0072
DD	0.0038 /0.00036	0.0044 /0.0004	0.0039 /0.0004	0.0057 /0.00045	0.0020 /0.0004	0.0027 /0.00048	0.0025 /0.0004	0.0028 /0.00041
PD	0.0013 /0.0002	0.0026 /0.0003	0.0012 /0.00034	0.0029 /0.00032	0.0014 /0.00037	0.0022 /0.0004	0.0019 /0.00026	0.0025 /0.0005
ES	0.0004 /0.0001	0.0014 /0.0005	0.00045 /0.00039	0.0018 /0.0012	0.00023 /0.00044	0.00088 /0.0016	0.00024 /0.00011	0.0008 /0.00067

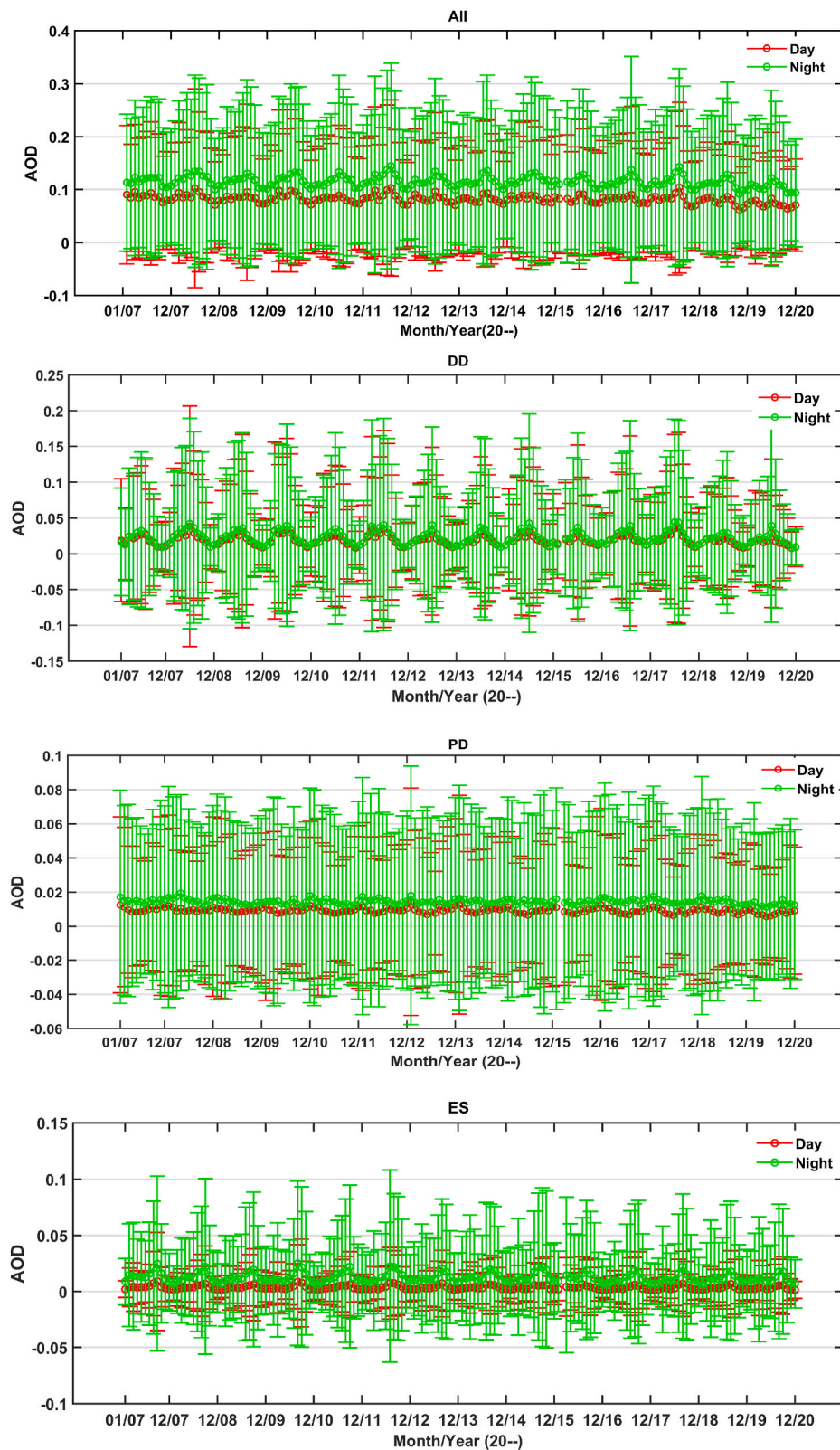


Fig. 9. Annual variations of mean AOD for All, DD, PD, and ES types of aerosols over the globe for the day and nighttimes during 2007–2019.

Table 3

The global inter-annual mean variations of AOD for different aerosol types during daytime and nighttime for the years 2007–2019.

Year	MAM		JJA		SON		DJF	
	Day	Night	Day	Night	Day	Night	Day	Night
2007	0.0834	0.1100	0.0177	0.0184	0.0098	0.0142	0.0042	0.0142
2008	0.0837	0.1146	0.0212	0.0243	0.0096	0.0151	0.0034	0.0151
2009	0.0798	0.1085	0.0184	0.0213	0.0091	0.0135	0.0034	0.0135
2010	0.0823	0.1112	0.0202	0.0223	0.0093	0.0136	0.0034	0.0136
2011	0.0791	0.1091	0.0173	0.0203	0.0090	0.0135	0.0033	0.0135
2012	0.0830	0.1133	0.0208	0.0233	0.0092	0.0141	0.0037	0.0141
2013	0.0795	0.1092	0.0172	0.0198	0.0094	0.0138	0.0032	0.0138
2014	0.0789	0.1090	0.0165	0.0189	0.0094	0.0138	0.0036	0.0138
2015	0.0812	0.1130	0.0197	0.0227	0.0088	0.0136	0.0033	0.0136
2016	0.0779	0.1070	0.0175	0.0199	0.0090	0.0133	0.0033	0.0133
2017	0.0791	0.1081	0.0194	0.0216	0.0087	0.0142	0.0029	0.0142
2018	0.0793	0.1094	0.0202	0.0237	0.0086	0.0137	0.0029	0.0137
2019	0.0755	0.1065	0.0170	0.0202	0.0087	0.0141	0.0034	0.0141

(58.93%) > DJF (56.21%). While for the ocean samples, it is JJA (34.90%) > MAM (31.34%) > DJF (24.45%) > SON (23.36%).

Over the NH and SH regions, the complexity of seasonal aerosol type variation reflects the significant impacts of both biomass burning emissions and desert on the aerosol composition in both regions. Besides, the clean marine (CM) aerosol appears to be the dominant type detected below 2 km in both NH and SH, due to a large oceanic area in this domain. Also, the mean aerosol EC for All aerosols decreased with the increase of height in all seasons in NH and SH. The maximum mean aerosol EC for All aerosols is 0.010 km^{-1} during the day in DJF in NH, while the maximum mean aerosol EC value is 0.006 km^{-1} during the day in JJA over the SH region for All aerosols. In general, the mean aerosol EC of all aerosol types for the nighttime in JJA over the NH are greater than those in other seasons; while the mean aerosol EC is the highest (except for PD) in SON over the SH. Overall, the annual and daily mean variations of global AOD for All and DD aerosol types have the same trend in deviation during the years 2007–2019. The AOD of total aerosol load showed an inter-annual decreasing trend, but a relatively stable seasonal variation.

Our analyses with the global aerosol optical data for more than a decade suggest the seasonal and diurnal variations of aerosol vertical and spatial distributions have qualitatively more reasonable and accurate in terms of extinction coefficient, AOD, and aerosol type, as well as maximum aerosol layer top altitude, compared to the previous versions. Our findings are favorable to improve and constrain the modeling of aerosols to play a key role in atmospheric dynamics and climate change.

Funding sources

This work was financially supported by the National Natural Science Foundation of China (Grant Nos. 42005074, 41888101), China Desert Meteorological Science Research Foundation (Grant No. Sqj2017014), the Strategic Priority Research Program of the Chinese Academy of Sciences (Grant No. XDA20100306), and the Start-Up Research Grant (SRG; File No. SRG/2020/001445) scheme sponsored by the Science and Engineering Research Board (SERB), a statutory body under the Department of Science and Technology (DST), New Delhi, India. One of the authors, KRK, is grateful to the DST, Govt. of India, for the award of the DST-FIST Level-1 (Grant No. SR/FST/PS-1/2018/35) scheme to the Department of Physics, KLEF.

CRedit author statement

All authors have read and agreed to the published version of the manuscript.

Conceptualization: H.P., J.H., and K.R.K.; Methodology: H.P.; Visualization and formal Analysis: H.P., J.Z., and L.A.; Validation: H.P., J.Z., and L.A.; Investigation: H.P.; Writing-original draft: H.P.; Writing-

review and editing: J.P., and K.R.K.; Supervision: J.H.; Project Administration: H.P.

Declaration of competing interest

The authors declare that they have no known competing financial interests or personal relationships that could have appeared to influence the work reported in this paper.

Acknowledgments

We are grateful to the CALIPSO (<https://eosweb.larc.nasa.gov/>) and MODIS (<https://ladsweb.modaps.eosdis.nasa.gov/>) instrument scientific teams at NASA for the provision of satellite data, which is available online and formed the central database in the present work. The authors would like to acknowledge Prof. James Jay Schauer, the Editor-in-Chief and Prof. Zhengqiang Li, Associate Editor of the Journal, and the four anonymous reviewers for their helpful comments and constructive suggestions towards the improvement of earlier versions of the manuscript.

References

- Butt, E.W., Rap, A., Schmidt, A., Scott, C.E., Pringle, K.J., Reddington, C.L., Richards, N. A.D., Woodhouse, M.T., et al., 2016. The impact of residential combustion emissions on atmospheric aerosol, human health, and climate. *Atmos. Chem. Phys.* 16, 873–905. <https://doi.org/10.5194/acp-16-873-2016>.
- Carslaw, K.S., Lee, L.A., Reddington, C.L., Pringle, K.J., Rap, A., Forster, P.M., et al., 2013. Large contribution of natural aerosols to uncertainty in indirect forcing. *Nature* 503, 67–71.
- Charlson, R.J., Schwartz, S.E., Hales, J.M., Cess, R.D., Coakley Jr., J.A., Hansen, J.E., et al., 1992. Climate forcing by anthropogenic aerosol. *Science* 255, 423–430.
- Chen, B., Huang, J., Minnis, P., et al., 2010. Detection of dust aerosol by combining CALIPSO active lidar and passive IIR measurements. *Atmos. Chem. Phys.* 10 (9), 4241–4251.
- Das, S., Harshvardhan, H., Bian, H., Chin, M., Curci, G., Protonotariou, A.P., et al., 2017. Biomass burning aerosol transport and vertical distribution over the South African-Atlantic region. *J. Geophys. Res. Atmos.* 122, 6391–6415. <https://doi.org/10.1002/2016JD026421>.
- Dayan, U., Ziv, B., Shoop, T., Enzel, Y., 2008. Suspended dust over South-Eastern Mediterranean and its relation to atmospheric circulations. *Int. J. Climatol.* 28 (7), 915–924. <https://doi.org/10.1002/joc.1587>.
- Fan, Yang, Huang, Jianping, He, Qing, et al., 2020. Impact of differences in soil temperature on the desert carbon sink. *Geoderma* 1370.
- Filonchik, M., Hurynovich, V., Yan, H., et al., 2020. Climatology of aerosol optical depth over Eastern Europe based on 19years (2000–2018) MODIS TERRA data. *Int. J. Climatol.* 40 (7).
- Heilman, W.E., Liu, Y., Urbanski, S., Kovalev, V., Mickler, R., 2014. Wildland fire emissions, carbon, and climate: plume rise, atmospheric transport, and chemistry processes. *For. Ecol. Manag.* 317, 70–79. <https://doi.org/10.1016/j.foreco.2013.02.001>.
- Hu, Z., Huang, J., Zhao, C., et al., 2019a. Trans-Pacific transport and evolution of aerosols: spatiotemporal characteristics and source contributions. *Atmos. Chem. Phys.* 19 (19), 12709–12730.
- Hu, Z., Huang, J., Zhao, C., et al., 2019b. Modeling the contributions of Northern Hemisphere dust sources to dust outflow from East Asia. *Atmos. Environ.* 202, 234–243. <https://doi.org/10.1016/j.atmosenv.2019.01.022>.

- Huang, J., Minnis, P., Yi, Y., et al., 2007. Summer dust aerosols detected from CALIPSO over the Tibetan Plateau. *Geophys. Res. Lett.* 34 (18), L18805.
- Huang, J., Minnis, P., Chen, B., Huang, Z., Liu, Z., Zhao, Q., Yi, Y., Ayers, J.K., 2008. Long-range transport and vertical structure of Asian dust from CALIPSO and surface measurements during PACDEX. *J. Geophys. Res.* 113, D23212. <https://doi.org/10.1029/2008JD010620>.
- Huang, J., Fu, Q., Su, J., et al., 2009. Taklimakan dust aerosol radiative heating derived from CALIPSO observations using the Fu-Liou radiation model with CERES constraints. *Atmos. Chem. Phys.* 9 (12).
- Huang, Z., Huang, J., Bi, J., Wang, G., Wang, W., Fu, Q., Li, Z., Tsay, S.-C., Shi, J., 2010. Dust aerosol vertical structure measurements using three MPL lidars during 2008 China-U.S. joint dust field experiment. *J. Geophys. Res.* 115, D00K15. <https://doi.org/10.1029/2009JD013273>.
- Huang, L., Jiang, J.H., Tackett, J.L., Su, H., Fu, R., 2013. Seasonal and diurnal variations of aerosol extinction profile and type distribution from CALIPSO 5-year observations. *J. Geophys. Res. Atmos.* 118, 4572–4596.
- Huang, J., Wang, T., Wang, W., Li, Z., Yan, H., 2014. Climate effects of dust aerosols over East Asian arid and semiarid regions. *J. Geophys. Res. Atmos.* 119 <https://doi.org/10.1002/2014JD021796>, 11,398–11,416.
- Huang, J., Liu, J., Chen, B., et al., 2015a. Detection of anthropogenic dust using CALIPSO lidar measurements. *Atmos. Chem. Phys.* 15 (20), 11653–11665.
- Huang, J., Wang, T., Wang, W., et al., 2015b. Climate effects of dust aerosols over East Asian arid and semiarid regions. *J. Geophys. Res. Atmos.* 119 (19), 11398–11416.
- Jia, R., Liu, Y., Chen, B., Zhang, Z., Huang, J., 2015. Source and transportation of summer dust over the Tibetan Plateau. *Atmos. Environ.* 123, 210–219. <https://doi.org/10.1016/j.atmosenv.2015.10.038>.
- Kaskaoutis, D.G., Kumar, S., Sharma, D., Singh, R.P., Kharol, S.K., Sharma, M., et al., 2014. Effects of crop residue burning on aerosol properties, plume characteristics, and long-range transport over northern India. *J. Geophys. Res. Atmos.* 119, 5424–5444. <https://doi.org/10.1002/2013JD021357>.
- Kumar, K.R., Kang, Na, Yin, Yan, 2018. Classification of key aerosol types and their frequency distributions based on satellite remote sensing data at an industrially polluted city in the Yangtze River Delta, China. *Int. J. Climatol.* 38 (1).
- Kumar, R.K., Sivakumar, V., Yin, Y., Reddy, R.R., Kang, N., Diao, Y., et al., 2014. Long-term (2003–2013) climatological trends and variations in aerosol optical parameters retrieved from MODIS over three stations in South Africa. *Atmos. Environ.* 95, 400–408. <https://doi.org/10.1016/j.atmosenv.2014.07.001>.
- Liu, D., Wang, Z., Liu, Z., Winker, D., Trepte, C., 2008. A height resolved global view of dust aerosols from the first year CALIPSO lidar measurements. *J. Geophys. Res.* 113, D16214. <https://doi.org/10.1029/2007JD009776>.
- Liu, Y., Zhu, Q., Huang, J., et al., 2019. Impact of dust-polluted convective clouds over the Tibetan Plateau on downstream precipitation. *Atmos. Environ.* 209, 67–77.
- Luo, Y., Zheng, X., Zhao, T., et al., 2013. A climatology of aerosol optical depth over China from recent 10 years of MODIS remote sensing data. *Int. J. Climatol.*
- Marinou, E., Amiridis, V., Biniotoglou, I., et al., 2017. Three-dimensional evolution of Saharan dust transport towards Europe based on a 9-year EARLINET-optimized CALIPSO dataset. *Atmos. Chem. Phys.* 17, 5893–5919.
- McKendry, I., Strawbridge, K., Karumudi, M.L., O'Neill, N., Macdonald, A.M., Leitch, R., Jaffe, D., Cottle, P., Sharma, S., Sheridan, P., Ogren, K., 2011. Californian forest fire plumes over southwestern British Columbia: lidar, sunphotometry, and mountaintop chemistry observations. *Atmos. Chem. Phys.* 11, 465–477. <https://doi.org/10.5194/acp-11-465-2011>.
- Mehta, M., Singh, N., Anshumali, 2018. Global trends of columnar and vertically distributed properties of aerosols with emphasis on dust, polluted dust and smoke - inferences from 10-year long CALIOP observations. *Rem. Sens. Environ.* 208, 120–132.
- Menzies, R.T., Tratt, D.M., 2002. Aerosol layers over the Pacific Ocean: vertical distributions and optical properties as observed by multi wavelength airborne lidars. *J. Geophys. Res.* 107 (D16), 4292.
- Mona, L., Amodeo, A., Pandolfi, M., Pappalardo, G., 2006. Saharan dust intrusions in the Mediterranean area: three years of Raman lidar measurements. *J. Geophys. Res. Atmos.* 111, D16203.
- Nan, Y., Wang, Y., 2018. De-coupling interannual variations of vertical dust extinction over the Taklimakan Desert during 2007–2016 using CALIOP. *Sci. Total Environ.* 633, 608–617.
- Omar, A.H., et al., 2009. The CALIPSO automated aerosol classification and lidar ratio selection algorithm. *J. Atmos. Ocean. Technol.* 26 (10), 1994–2014. <https://doi.org/10.1175/2009JTECHA1231.1>.
- Pan, B., Liu, D., Kumar, K.R., et al., 2021. Global distribution of maritime low clouds with an emphasis on different aerosol types and meteorological parameters inferred from multi-satellite and reanalysis data during 2007–2016. *Atmos. Environ.* 246, 118082. <https://doi.org/10.1016/j.atmosenv.2020.118082>.
- Pan, H., Wang, M., Kumar, K.R., et al., 2019. Seasonal and vertical distributions of aerosol type extinction coefficients with an emphasis on the impact of dust aerosol on the microphysical properties of cirrus over the Taklimakan Desert in Northwest China. *Atmos. Environ.* 203, 216–227.
- Pan, H., Huo, W., Wang, M., et al., 2020. Insight into the climatology of different sand-dust aerosol types over the Taklimakan Desert based on the observations from radiosonde and A-train satellites. *Atmos. Environ.* 238 <https://doi.org/10.1016/j.atmosenv.2020.117705>, 117705, ISSN 1352-2310.
- Rashki, A., Kaskaoutis, D.G., Eriksson, P.G., de W Rautenbach, C.J., Flamant, C., Abdi Vishkaee, F., 2014. Spatio-temporal variability of dust aerosols over the Sistan region in Iran based on satellite observations. *Nat. Hazards* 71, 563–585.
- Roberts, G., Wooster, M.J., Lagoudakis, E., 2009. Annual and diurnal African biomass burning temporal dynamics. *Biogeosciences* 6, 849–866. www.biogeosciences.net/6/849/2009/.
- Schuster, G.L., Vaughan, M., MacDonnell, D., Su, W., Winker, D., Dubovik, O., et al., 2012. Comparison of CALIPSO aerosol optical depth retrievals to AERONET measurements, and a climatology for the lidar ratio of dust. *Atmos. Chem. Phys.* 12, 7431–7452. <https://doi.org/10.5194/acp-12-7431-2012>.
- Shikwambana, L., Sivakumar, V., 2018. Global distribution of aerosol optical depth in 2015 using CALIPSO level 3 data. *J. Atmos. Sol. Terr. Phys.* 173 <https://doi.org/10.1016/j.jastp.2018.04.003>.
- Sogacheva, L., Popp, T., Sayer, A.M., et al., 2020. Merging regional and global aerosol optical depth records from major available satellite products. *Atmos. Chem. Phys.* 20 (4), 2031–2056.
- Solanki, R., Singh, N., 2014. LiDAR observations of the vertical distribution of aerosols in free troposphere: comparison with CALIPSO level-2 data over the central Himalayas. *Atmos. Environ.* 99, 227–238.
- Tandule, C.R., Kalluri, R.O.R., Gugamsetty, B., et al., 2020. Decadal climatology of the spatial and vertical distributions of tropospheric aerosol over the Arabian Sea based on satellite observations. *Int. J. Climatol.* <https://doi.org/10.1002/joc.6482>.
- Textor, C., Schulz, M., Guibert, S., Klne, S., Balkansk, Y., Bauer, S., et al., 2006. Analysis and quantification of the diversities of aerosol life cycles within AeroCom. *Atmos. Chem. Phys.* 6, 1777–1813.
- Uno, I., Amano, H., Emori, S., Kinoshita, K., Matsui, I., Sugimoto, N., 2001. Trans-Pacific yellow sand transport observed in April 1998: a numerical simulation. *J. Geophys. Res.* 106 (D16), 18,331–18,344.
- Uno, I., Yumimoto, K., Shimizu, A., Hara, Y., Sugimoto, N., Wang, Z., Liu, Z., Winker, D.M., 2008. 3D structure of Asian dust transport revealed by CALIPSO lidar and a 4DVAR dust model. *Geophys. Res. Lett.* 35, L06803. <https://doi.org/10.1029/2007GL032329>.
- Vaughan, G., Draude, A.P., Ricketts, H.M.A., Schultz, D.M., Adam, M., Sugier, J., Wareing, D.P., 2018. Transport of Canadian forest fire smoke over the UK as observed by lidar. *Atmos. Chem. Phys. Discuss.* <https://doi.org/10.5194/acp-2017-1181>.
- Wang, X., Huang, J., Ji, M., Higuchi, K., 2008. Variability of East Asia dust events and their long-term trend. *Atmos. Environ.* 42, 3156–3165. <https://doi.org/10.1016/j.atmosenv.2007.07.046>.
- Wang, T., Han, Y., Huang, J., Sun, M., Jian, B., Huang, Z., Yan, H., 2020. Climatology of dust-forced radiative heating over the Tibetan Plateau and its surroundings. *J. Geophys. Res. Atmos.* 125, e2020JD032942 <https://doi.org/10.1029/2020JD032942>.
- Winker, D.M., et al., 2006. The CALIPSO mission and initial results from CALIOP. *Proc. SPIE* 6409, 640902.
- Winker, D.M., Tackett, J.L., Getzewich, B.J., Liu, Z., Vaughan, M.A., Rogers, R.R., 2013. The global 3-D distribution of tropospheric aerosols as characterized by CALIOP. *Atmos. Chem. Phys.* 13, 3345–3361. <https://doi.org/10.5194/acp-13-3345-2013>.
- Yu, H., Chin, M., Winker, D.M., Omar, A.H., Liu, Z., Kittaka, C., Diehl, T., 2010. Global view of aerosol vertical distributions from CALIPSO lidar measurements and GOCART simulations: regional and seasonal variations. *J. Geophys. Res.* 115, D00H30. <https://doi.org/10.1029/2009JD013364>.
- Zhang, Z., Huang, J., Chen, B., et al., 2019. Three-year continuous observation of pure and polluted dust aerosols over northwest China using the ground-based lidar and sun photometer data. *J. Geophys. Res. Atmos.* <https://doi.org/10.1029/2018JD028957>.